Acta Astronautica 118 (2016) 224–236

Contents lists available at ScienceDirect

Acta Astronautica

journal homepage: www.elsevier.com/locate/actaastro

A spaceborne, pulsed UV laser system for re-entering or nudging LEO debris, and re-orbiting GEO debris

Claude R. Phipps [a,*], Christophe Bonnal [b]

[a] Photonic Associates, LLC, Santa Fe, NM 87508 USA
[b] CNES Launcher Directorate, 75012 Paris, France

ARTICLE INFO

Article history:
Received 1 September 2015
Accepted 7 October 2015

Keywords:
Geosynchronous orbit
Space debris removal
Laser ablation
Laser-produced plasma
Ultraviolet lasers
Laser-surface interaction

ABSTRACT

Among the problems raised by the presence of debris in Earth Orbit, the question of large derelict satellites in Geostationary Orbit (GEO) is of major importance. More than 1000 defunct GEO satellites cruise in the vicinity of this unique orbit and pose the question of orbital slot availability.

It is proposed to use lasers in GEO to reorbit the large debris in the graveyard zone, some 300 km above GEO. The principle of orbital transfer by laser ablation is recalled, and two different methods are described. These lasers can also serve for small debris deorbiting and large debris nudging in Low Earth Orbit (LEO). Technical details are provided, as well as a preliminary mass budget.

1. Introduction

The number and mass of artificial objects in Earth Orbit are increasing steadily since 1957 [1].

Some 23k objects larger than 10 cm are detected, out of which 17k are tracked [2], more than 500k objects larger than 1 cm, and more than 100 million debris larger than 1 mm are also identified. These artificial objects amount to nearly 7000 ton spread above our heads, comparable to the mass of the Eiffel Tower.

The number of debris increases mainly in Low Earth Orbit (LEO) with an altitude of perigee lower than 2000 km at any inclination, but it increases significantly in the vicinity of Geostationary Orbit (GEO), defined as 35786 ± 200 km altitude $\pm 15°$.

This increase in number and mass may be troublesome, as it is observed despite a significant reduction in the number of launches compared to the years 70–80, and despite the progressive adoption of mitigation rules since the 1995–2002 period (NASA standard in 1995, JAXA standard in 1997, CNES standard in 1999, IADC Guidelines in 2002, UN Guidelines in 2007, ISO 24113 in 2011 and so on…).

2. Problems associated with debris in orbit

The artificial objects in orbit can be distributed following 5 categories, defined by size and orbits, each corresponding to specific concerns and solutions.

2.1. Active satellites

Some 1100 to 1200 satellites are operational in orbit. The main concern is economic, associated with collisions in orbit which would lead to the loss of the operational status of very valuable spacecraft. The specific case of manned spacecraft, anecdotic, can be emphasized.

These satellites are cataloged, with precise ephemeris; in most cases, they are maneuverable, either thanks to a propulsion system, or in some cases thanks to an attitude

* Corresponding author.
E-mail addresses: crphipps@photonicassociates.com (C.R. Phipps), christophe.bonnal@cnes.fr (C. Bonnal).

http://dx.doi.org/10.1016/j.actaastro.2015.10.005
0094-5765/

change enabling a modification of their drag leading to a slight orbital modification.

The specific case of very small satellites, such as cubesats, often launched in swarms, may generate unexpected problems. Current simulations led at international level do not yet take them into account and their effect on the long-term orbital evolution is not yet understood.

The majority of these satellites can perform Collision Avoidance Maneuvers. Such operations are heavy, imply significant manpower, but are now quite classical, through the Conjunction Assessment Reports issued by JSpOC in US [3], augmented by dedicated post-treatment and decision process such as the CAESAR service proposed by CNES [4]. The future of such operations may be questioned when considering the expected drastic increase in the number of cataloged objects in the future, due to improved sensors planned to operate in 2018. This question is not addressed in the present paper.

2.2. Large integral debris in Low Earth Orbits

There are more than 4000 large integral objects with perigee altitude lower than 2000 km, defunct satellites or upper stages left in orbit.

They may act as important sources of small debris following collisions with other debris, even small ones. A collision with a 1 cm debris, at orbital velocity, represents an energy in the order of magnitude of 1 MJ and can generate thousands of new debris, themselves prone to further collisions. Such a cascading effect may be slow, its effect measurable only after decades, but if it generates debris at a rate larger than the natural orbital cleansing due to residual atmosphere, the process may become divergent (so-called Kessler syndrome [5]).

These large debris are cataloged, but are not maneuverable. There is currently no detection process assessing detailed collision risk, as is done for active spacecraft, since it would require a huge effort to take into account all cataloged objects, and since anyhow there is no way to avoid such collisions.

Numerous ideas have risen aiming at reducing this cascading effect by removing some of the most critical debris from the most critical orbits [6]. An abundant literature describes all the options for Active Debris Removal, with numerous variants for chasers, rendezvous procedures, interfacing systems (robotic arms, nets, harpoons…), and various deorbiting systems, either passive (drag augmentation devices), conventional propulsive systems or more innovative ones (Electro Dynamic Tethers) [7].

One option has been proposed by several scientists, consisting in imparting a slight trajectory modification to one of the two large debris slightly before an expected collision; such “nudging” has been proposed by various authors [8], based for instance on the creation of an “artificial atmosphere” in front of one of the debris to increase the drag.

Space-borne lasers could be used efficiently to perform such nudging [9]. This solution is described briefly in the following paragraphs.

2.3. Cataloged smaller debris in Low Earth Orbits

There are more than 10k relatively small debris cataloged in Low Earth Orbits, with sizes typically larger than 10 cm.

They have the ability to destroy active satellites, or at least to disable them functionally, the kinetic energy associated to a collision being such that it generates significant local damage. The associated probability of collision, a function of their cross-section, is low, so the effect on orbital population is feared only in the long term. However, integrated over decades, it leads to debris regeneration and satellite loss.

Unfortunately, there is currently no way to avoid collision between such debris and larger objects. Large operational satellites may avoid collision, as seen in §2.1, but others are defenseless.

If laser debris removal options were efficient for smaller debris, and if progress in the domain would enable it, one could imagine at long term to use such solutions to get rid of this class of impactors, but removal of the larger ones of these may not be technically credible yet.

2.4. Small un-cataloged debris in Low Earth Orbits

The smaller debris in Low-Earth Orbits, with sizes ranging from 1 cm to 10 cm, represent nearly a million potential impactors, potentially capable of damaging active satellites, leading to loss of function following collisions.

Several studies have shown that the probability of loss of function of an active satellite in the most densely populated orbits may reach several percent over the lifetime of the spacecraft; the economic loss may become significant. This is also true for the International Space Station, because of its huge cross-section.

Contrarily to other cases, the feared effect here is not a long term one, but much more a short one, with risks to damage an operating satellite during its functioning lifetime.

Satellites can be shielded, and there is a wide range of solutions generally based on the addition of several layers of material, such as Kevlar® bumper, separated by standoffs, in front of critical zones [10]. Unfortunately, the efficiency of such shields decreases with the size of the impactor, with a limit in the range of 1 cm.

So far, there have been no credible solutions to get rid of this population of very small debris: they are not tracked, and our knowledge is mainly statistical. The only sound solutions studied so far is the laser sweeper, either from ground or orbited.

2.5. Large integral debris in Geostationary Orbit

Last, we consider large derelict satellites in the vicinity of the GEO belt, including some large upper stages, which is a completely different problem.

There are typically 1000 such objects in addition to the 440 controlled (active) satellites, which is a relatively low number when considering the size of the GEO belt (Fig. 1 [11]). There is no problem of debris density, and no real

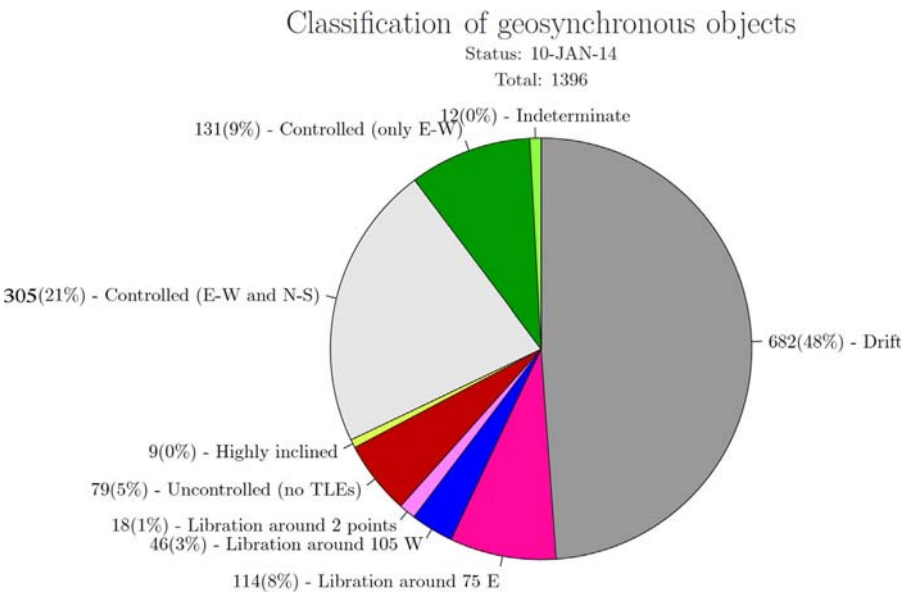

Fig. 1. Number of objects in GEO per category.

risk of collision; in case of a collision, anyhow, the relative velocity would be relatively low (500 m/s compared to up to 15 km/s in LEO), so the effects would most probably not be "catastrophic".[1]

The main problem in GEO is the occupation of valuable slots by derelict satellites, a situation similar to a parking lot with numerous valuable slots occupied by wrecked abandoned cars.

It is a short-term problem, as there is often an immediate need to free an orbital slot for a new satellite, or a relocated satellite following a change of operational region. Worse, 48% of the objects left in drift orbit regularly cross GEO, twice a day, as seen on Fig. 2 [11].

Ideally, one would need to increase the orbit of the debris to reach the GEO graveyard zone, roughly 300 km above the GEO arc.

Some solutions have been proposed, generally derived from LEO Active Debris Removal (§2.2) [12], described in more detail in the following section.

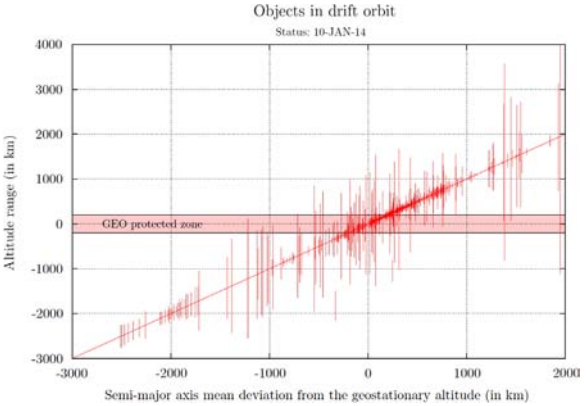

Fig. 2. Distribution and altitude range of the objects in drift orbit.

3. Laser debris removal

3.1. Brief review of the past and current studies on laser debris removal

Debris removal thanks to laser–matter interaction has been studied since more than 25 years now, and is still subject to numerous studies throughout the world.

Historically, these ideas were directly derived from the concepts of laser propulsion, such as those published by Kantrowitz in 1986 [13] during a dedicated workshop organized by DARPA, even though one can quote earlier works associated with photonic propulsion (Sänger, Marx, Möckel, Kantrowitz).

The first ideas related to laser–matter coupling aimed at producing an impulse on the target were published by Phipps in 1988 [14], giving the interaction theory supported by an extensive survey of existing experimental results. This was completed in 1994 with the LISK-BROOM concept [15]; this idea already included the nudging of large debris in order to avoid orbital collisions.

Based on these ideas, Schall [16] from DLR presented in 1990 a theoretical idea, derived from laser propulsion results published in 1986, associated to some preliminary experiments; the idea of a space-based laser was then already identified.

The most complete study, by far, was the ORION project aimed at cleaning the ISS orbit from its small debris thanks to a large laser on ground. Orion was a NASA headquarters study, first published [17] by Phipps and scientists from LLNL, LANL and other institutions; then, in far more detail as a NASA Technical Memorandum in 1996 by Campbell

[1] In the debris world, catastrophic failure is taken to result from a collision with kinetic energy >55 kJ/kg of target mass.

[18]. In one of its last versions, it consisted of a large 20 kW ground based laser, $\lambda = 530$ nm. After a very significant project effort, it was not pursued further.

More recently, an EU study called Cleanspace [19] gave very good results, considering the coupling and the phasing of several lasers in parallel and testing it with success for up to 9 lasers.

Nudging debris in order to avoid collision was studied by Stupl et al. from NASA Ames in 2013 [20].

Chinese scientists have recently published a proposal for a space based laser sweeper [21] with $\lambda = 1.06$ μm and a pulse duration of 7 ns; with a 2.4 diameter mirror, the far spot size is 15 cm in diameter.

Schmitz, from Airbus Defence & Space, presented in 2013 a concept of laser sweeping from orbit [22].

A recent announcement from Australian researchers from RMIT in Melbourne described a laser debris removal system planned from Mt Stromlo.

Researchers from LLNL in the US have published in 2010 based on practical experience coming from the NIF laser [23]. Then in 2012, Phipps and coauthors from LLNL, SNLA and three other institutions published an overview of laser orbital debris removal (LODR) by an Earth-based laser station. For the first time, this included a detailed assessment of ion charge states in laser induced momentum coupling, laser orbit modification for general non-circular orbits, optical constraints on the beam from passing through the atmosphere, target shape effects, and totally automatic Brillouin-Enhanced Four-Wave Mixing (BEFWM) as a possible adjunct to active target tracking [24].

The most recent initiative appears to be the proposal to use the future ICAN laser (International Coherent Amplifying Network) to sweep small debris from LEO. This laser, based on massively parallel coherent fiber lasers, using as many as 100k individual fiber lasers, would theoretically be capable of delivering huge energies on very small targets [25,26]. A first demonstration with a prototype small CAN laser is expected to fly on ISS in 2018. These colleagues organized a successful workshop in Paris devoted to "Laser Solutions for Orbital Debris" [27].

This rapid survey of the topic is not exhaustive by far, and has no intention to be so.

It only aims at showing how the ideas have evolved over the last 25 years, and the impressive number of studies currently going on that topic. The present paper aims at taking into account all these past studies to build an optimal proposal.

3.2. Physical principle

When irradiated above a given fluence threshold (J/m²), materials tend to vaporize. Heating of the material can be very fast, followed by creation of plasma which is ejected at high velocity, roughly perpendicularly to the surface. It is important to choose a laser pulse with an appropriate duration: too short, it would create no vapor or plasma and therefore no impulse. Pulses longer than optimum heat up the plasma unnecessarily; longer pulses yet (in the ms range) melt deeply, cause splashing and create more debris.

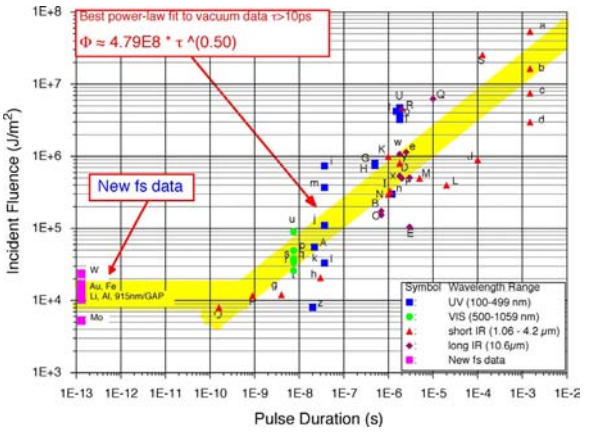

Fig. 3. Optimal fluence of a pulse as a function of pulse duration.

Optimum fluence is usually just above the transition to plasma. Fluence above this level is increasingly inefficient in producing target momentum because $C_m v_E$ is a product limited by energy conservation, and laser energy is going into increasing ejection velocity v_E at the expense of C_m, the efficiency of laser pulse energy in producing momentum on a target by ablation.

A theoretical curve has been established, based on some 43 experimental results, establishing the optimum plasma formation threshold of a pulse as a function of its duration: a value of 100 ps appears to be the best, as shown in Fig. 3 from Phipps [28].

A coupling factor C_m can be defined in terms of radiation parameters. It varies with the intensity of the irradiation I (W/m²), wavelength λ and the duration of the pulse τ (s) according to [14]:

$$C_m \rightarrow C_{mo}/(I\lambda\sqrt{\tau})^{1/4} \quad (1)$$

for large $I\lambda\sqrt{\tau}$ and pulses longer than 100 ps. C_{mo} is primarily a function of the average atomic mass A and charge state Z in the laser produced plasma above the surface. Clearly, (1) diverges to infinity for $I \rightarrow 0$. More carefully derived theoretical values of C_m near the plasma transition intensity, show a C_m maximum, as it must, matching the results of tests on several materials are shown in Fig. 4 [29]. Obtaining the results of Fig. 4 requires difficult modeling, but Fig. 3, also based on lots of data, gives a good estimate of the peak value. For designing systems with high confidence of igniting all materials, we choose a value for $\Phi_{opt}/\sqrt{\tau} = I_{opt}\sqrt{\tau} = 8.5E8$ W/m² s$^{1/2}$, 75% larger than the trend. Then $(I\lambda\sqrt{\tau})_{opt} = 850\lambda_{\mu m}$ Wm$^{-1}\sqrt{s}$. For a best theoretical estimate of typical C_m, we retain Fig. 3 value, with $(I\lambda\sqrt{\tau})_{opt} = 480\lambda_{\mu m}$ Wm$^{-1}\sqrt{s}$.

By combining this best estimate with Eq. (1), we have obtained a surprisingly good estimate of maximum C_m:

$$C_m \approx 0.21 C_{mo} \lambda_{\mu m}^{-1/4} \text{N/W}. \quad (2)$$

For aluminum with a singly ionized plasma, $C_{mo} \approx 460$ N/MW. We can specify some parameters in advance. Eq. (2) suggests using the smallest possible wavelength consistent with optical damage of laser components for the best momentum coupling. We select the

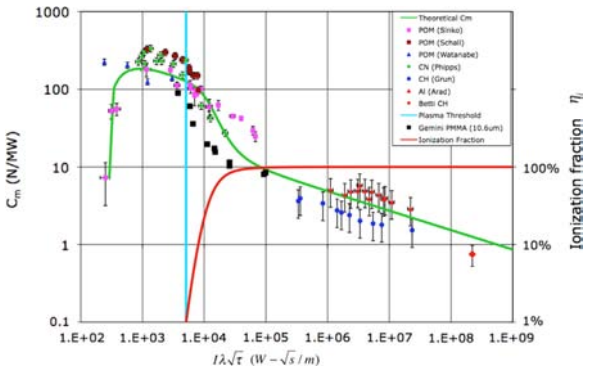

Fig. 4. Coupling coefficient as a function of the pulse characteristics. Red line is ionization fraction. (For interpretation of the references to color in this figure legend, the reader is referred to the web version of this article.)

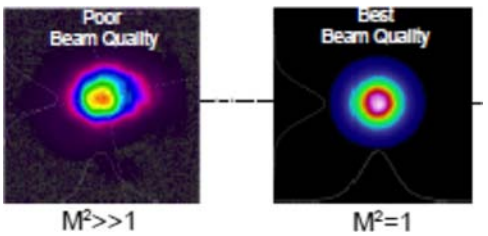

Fig. 5. Beam quality.

3rd harmonic of Nd:YAG at $\lambda=355$ nm (UV laser) because optical damage thresholds for the laser components dive rapidly at shorter wavelengths. For $\lambda=355$ nm, Eq. (2) leads to a realistic peak value of $C_m=128$ N/MW, a value well supported by data on aluminum at other wavelengths [31].

These choices have numerous advantages: UV can be propagated from a spacebased system, is absorbed by materials much more efficiently than longer wavelengths, gives more momentum coupling (Eq. (2)), and the beam focal spot size due to diffraction is 3 times smaller than with the fundamental harmonic at $\lambda=1064$ nm, given the classical diffraction formula Eq. (3):

$$r_o \rightarrow \frac{2M^2\lambda L}{\pi D} \text{ in the limit } L \gg D \tag{3}$$

In Eq. (3), L is distance from a transmitting aperture with diameter D to the target and r_o is the spot radius there. M^2 is the beam quality, where $M^2=1$ is the best achievable. It is the inverse of the Strehl ratio [please see Appendix 2 for the exact result]. Fig. 5 illustrates beam quality [30].

Last, one has to check that for a given distance L_{max}, the pulse energy E_L generates the optimal fluence Φ_{opt} required for the proper operation of laser ablation. Eq. (3) gives

$$L_{max} = \sqrt{\frac{\pi E_L}{\Phi_{opt} 2M^2\lambda}}\, D \tag{4}$$

It may be useful here to give some numerical orders of magnitude: a 100 J pulse hitting a larger target perpendicularly with a spot radius of 6 cm generates a fluence Φ of 8.5 kJ/m². If the pulse has a duration $\tau=100$ ps, the intensity I on the target is 85 TW/m²! The associated erosion of the target is on the order of 20 nm. With $C_m \approx$ 100 N/MW, we expect an impulse of 10 mN s, and a pressure of 8.5 GN/m², or 85 kbar. To generate this pressure, the corresponding ejection velocity of a 20 nm layer of aluminum must be 16 km/s and specific impulse I_{sp} is 1670 s. The product $C_m I_{sp}=0.17$, close to the theoretical value. For a 1 m diameter mirror using a third harmonic beam with $M^2=2$ (very realistic), we expect $L_{max}=137$ km, which is largely sufficient.

3.3. L'ADROIT laser orbital debris remover

L'ADROIT (Laser Ablative Debris Removal by Orbital Impulse Transfer…), is a spacebased debris removal system described in Ref. [31].

Solar powered, it consists of two telescopes:

1. One for target acquisition, a wide field of view (60°) passive sensor identifying targets using solar illumination thanks to a very specific design based on two conical mirrors, adapted from Köse and Perline [32]. The array detector has 220 M pixels, leading to 70 μrad/pixel.
2. One for laser operation with 6 mrad narrow field of view for active acquisition and firing; it tracks the target, obtains returns from it, focuses on it and fires repeatedly to alter its orbit. Because the outgoing pulse is polarized, it passes through the splitter with zero loss, while the return pulse suffers a 50% loss. Only the active telescope is steered. The off-axis Cassegrain design permits using a larger secondary mirror without causing obstruction. A zoom lens pair lets us match beam waist to target position. The detector is 9 M pixel, leading to 2 μrad/pixel (Fig. 6).

3.4. Application to GEO debris removal

Once these parameters are clarified, an application to GEO debris removal can be established.

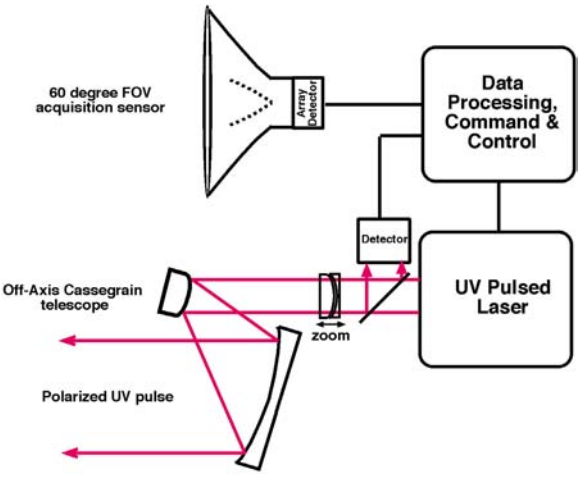

Fig. 6. L'ADROIT laser orbital debris remover.

We consider an orbital laser functioning at 3rd harmonic of Nd:YAG at $\lambda = 355$ nm, delivering 500 J pulses with pulse duration $\tau = 100$ ps (Figs. 7–9).

The 500 J hypothesis enables to keep relatively small optics. A classical figure for 355 nm optics is 3 J/cm²; considering a conservative value of 1 J/cm², it leads to optics which could be as small as 25 cm in diameter.

The laser is located at 10 km west of the target, following it; the impulses imparted by the laser will therefore tend to increase the altitude of the debris.

Delivered fluence is 8.5 kJ/m² as described previously; the size of the spot is made to be 27 cm by deliberate defocusing. A coupling coefficient $C_m = 100$ N/MW is assumed, leading to an impulse $J = 50$ mN s per pulse.

If we consider a very large derelict GEO satellite as a target, with a mass $M = 3$ ton (which is close to be the worst case), the average Δv per pulse is $J/M = 17$ μm/s. During the active phase of the laser, with a PRF = 64 Hz, the average acceleration of the target is 1.1 mm/s².

The debris has to be reorbited by at least 300 km, which represents a total $\Delta v = 11$ m/s. This corresponds to 650 k pulses, or a total laser operation duration of 14.2 h.

3.4.1. Flight profile – variant A

The laser has to follow the target during all its ascent phase.

Furthermore, the raising of the debris orbit cannot be done in 3 or 4 h but should take more than 12 h in order to end up with a circular orbit.

To that extent, the chaser is equipped with an electrical propulsion system consisting in 2 Snecma PPS-5000-E-2G Hall Effect Thrusters. When electrically fed with a power of 5 kW, such thrusters deliver a maximum thrust of 240 mN with a specific impulse of 2150 s.

The operation of the chaser is bi-modal: it uses the onboard electrical power to feed the laser during the active phases, and to correct its altitude and follow the target during the rest of the time.

We consider here that the laser is used 20% of the time, so the average power required by the laser during the complete operation will be 25 kW.

We assume for instance that the chaser is equipped with a Solar Generation System delivering 36 kW, q in line with current studies for evolved GEO spacecraft; out of these 36 kW, 25 kW will be used permanently for the laser, in a cycle where 80% of the time is used to charge super capacitors, with laser off, and 20% of the time is used discharging the super capacitors, and providing the laser with its full power.

The other 11 kW are used to feed the 2 electrical engines of the chaser (10 kW) and to feed the other equipment of the chaser (1 kW for telecommunications, GNC, torquers, thermal control…).

The propulsion system has to provide a $\Delta v = 11$ m/s to reach the GEO graveyard zone following the debris, so the total consumption in Xenon would be 1.3 kg, for the ascent, and 1.3 kg to come back to GEO after the operation (one can note that significant activities are currently ongoing to adapt these engines to Krypton or Argon in the future, much less expensive).

During the laser burst, the thrust imparted to the debris is 3.2 N; the laser is used during 20% of the time, so the average thrust imparted to the debris is 640 mN, similar to the total thrust provided by the two electrical engine of the chaser: indeed, the two objects are “co-orbiting” at a

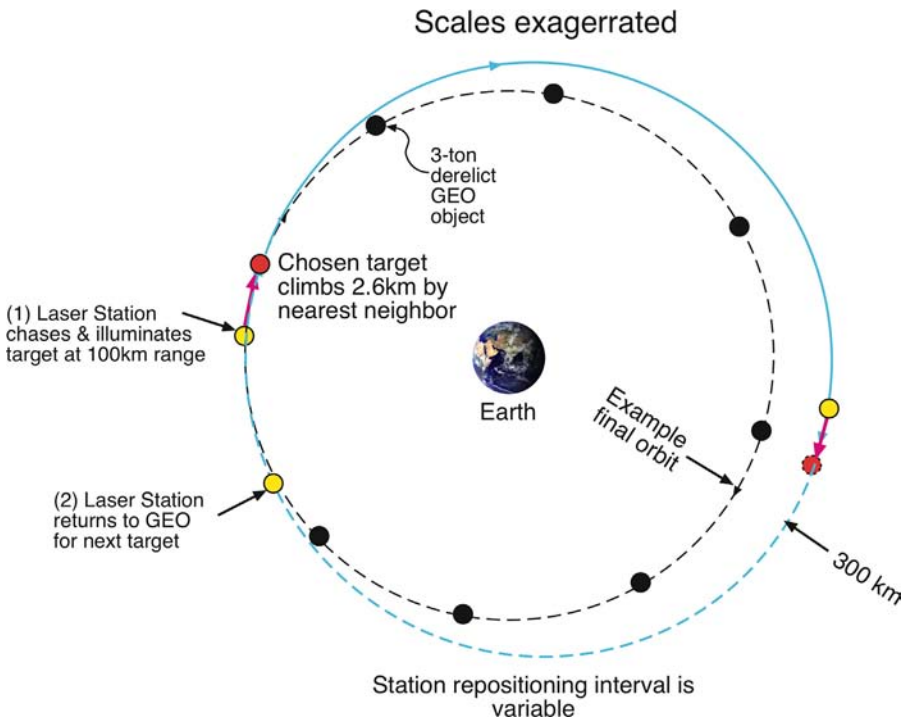

Fig. 7. GEO reorbiting variant A: single chaser.

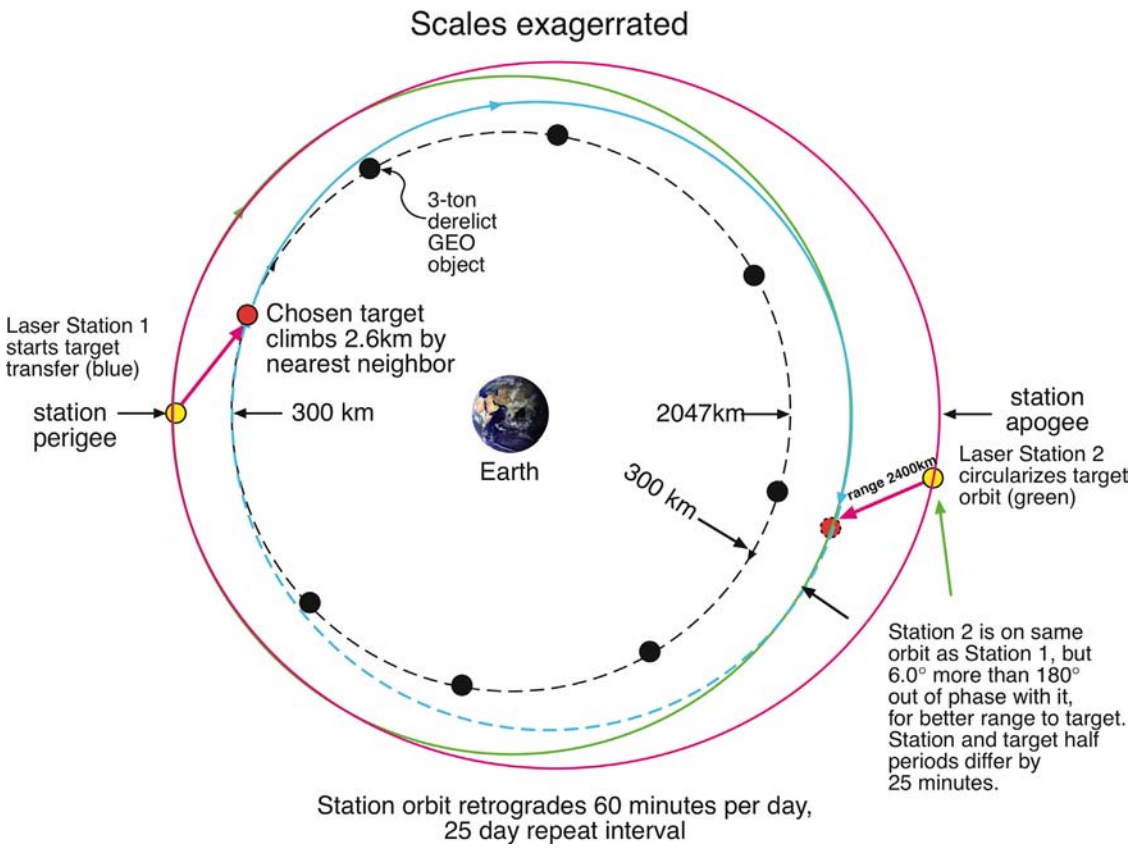

Fig. 8. GEO reorbiting variant B: two chasers.

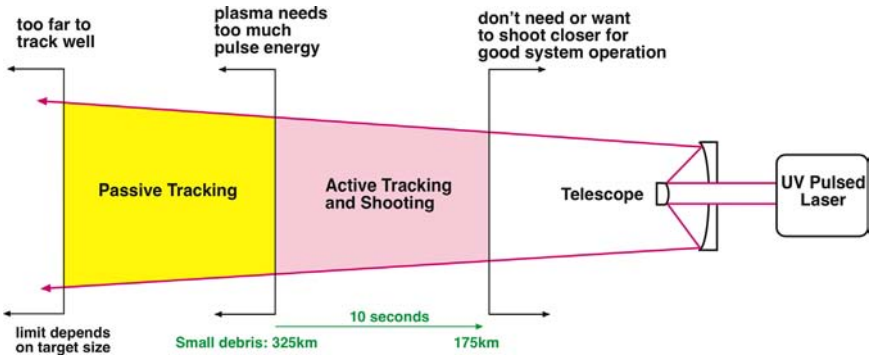

Fig. 9. Small debris removal in LEO.

relatively constant distance of 10 km during the complete ascent phase. This phase lasts 14 h, followed by the return of the chaser in GEO, which takes another 16 h after which the system is ready to go and engage its next target (longitude drift above or below GEO to reach the proper point, then positioning 10 km West of the new target).

If the target is lighter than considered here (3 ton), the proportion of time during which the laser is used would be reduced, as well as the feeding power to the two electrical engines (as was demonstrated on the Snecma PPS-1350 engine used for the Smart-1 mission); indeed, the power and the proportion of active use of the laser can be regulated to guarantee a very effective coorbitation of the two objects during ascent.

3.4.2. Inclined orbits

In the non-ideal case, the debris are not in GEO with a 0° inclination, but may cruise in the vicinity of GEO following a slightly elliptical orbit with inclination potentially reaching up to 15°, worst case of the N/S cycle induced by Luni-Solar perturbations.

The eccentricity of the orbit has no significant effect on the dimensioning of the chaser; it shall be correctly located at the beginning of the operations to be co-orbiting

with the debris, but there is no effect on Xenon mass or on mission duration.

The effect of inclination is much more significant.

Here again, the chaser will perform a rendezvous with the debris prior to the beginning of the relocation operations. In the worst case of an inclination of 15°, the corresponding Δv would be 780 m/s. During this rendezvous phase, the laser is not used, so one can take benefit of the full power of the chaser; a 3rd HET engine is mounted, enabling a total thrust of 720 mN. The ascent phase leads to a Xenon consumption of 75 kg, to which 75 kg shall be added to return to GEO after the debris reorbiting.

The transfer duration becomes 25 days for ascent, and 25 days for descent, so globally roughly 2 months for the complete operation.

This corresponds to the worst possible case, as most of the debris have inclinations significantly less than 15°, and a global optimization of the debris sequence could be performed.

As a synthesis, one can imagine a 2.5 ton chaser equipped with a L'ADROIT laser, with Solar Generators providing 36 kW power, dimensioned for 10 debris, each of a maximal mass of 3 ton, including 2 debris at 15° inclination. The total consumption in Xenon (or Krypton) over the complete lifetime (including re-orbiting of the chaser itself!) would be 320 kg, and the complete duration of mission would be in the range of 2 years. Lighter debris or lower inclinations would of course improve the global performance of the system.

3.4.3. Variant B with two chasers

The operational scheme described in the previous section is efficient and fast, but leads potentially to a high propellant consumption, which may turn out to be the limiting factor for the operational lifetime of the chaser.

A variant B is proposed considering two chasers located on the same elliptical orbit, with perigee altitude 300 km above GEO, and apogee altitude 2047 km above GEO; the two chasers are 180° from each other. This orbit compared to GEO is slightly retrograde; its period is 3485 s longer than the GEO period, meaning that any of the two stations retrogrades by 10720 km per day, leading to a 24.7 day repeat interval.

It means that every 25 days, the two chasers will be in the vicinity of every debris in GEO (there is no perigee drift, the argument of perigee deprival being excessively small, needing some 40 years to do a complete revolution..).

The operations can be seen as some volleyball game!

The first station raises the apogee of the debris, then the second station tends to circularize it. The operations are progressive, raising each time by some 100 km, thus requiring a total of 75 days to reorbit one debris. But during these 75 days, the system can engage with much more than just one debris, as every debris will pass 3 times in front of each station in this interval of time. Practically, the system can address continuously the complete orbital debris population, up to a given inclination (estimated to be 3.4°, but this value should be refined).

The main advantage of this variant is that the chasers do not need to perform any orbital transfer, so the Xenon consumption is basically negligible; the only maneuver required is the proper orientation in order to align correctly the laser beam with the targeted spot on the debris.

There are several drawbacks though: since the distance between the laser and the debris is relatively large, hundreds or thousands of kilometers, the sizing of the laser and transmitting mirror have to increase; considering a maximal range of 2400 km, a 3 m diameter mirror is required. Pulses have also to be more energetic, with a typical 6.8 kJ pulses, leading to target acceleration of 230 μm/s/pulse.

3.5. Application in LEO

The system described here can be used for two other applications in LEO.

3.5.1. Small debris removal in LEO

As already published in [31], the L'ADROIT system can be used to solve the problem of small un-tracked objects in LEO.

As a typical example, a 50 g debris on a circular orbit at 760 km altitude can be deorbited in one single path of 10 s with a 2-minute down time for heat dissipation. The required Δv is 160 m/s. Considering an average range of 250 km, an efficiency $\eta = 0.8$ and an energy density $\Phi = 8.5$ kJ/m² (as seen previously), it requires 2300 pulses at 83 J, with a Pulse Repetition Frequency of 120 Hz over 10 s. The average laser electrical power is just 3.2 kW and we consider a 3 m diameter mirror, very conservative.

The debris sweeper could engage small debris in a nearly permanent profile, meaning more than 100 k debris per year…

3.5.2. Large debris nudging in LEO

The system can be used for "Just In Time" collision avoidance, slightly deflecting the trajectory of a large debris prior to a predicted collision, or more pragmatically, improving the probability of such a collision.

As a typical example, we consider the avoidance of a collision by 10 km, 2 due to altitude variation, 8 due to change in orbital period. Considering debris on a circular orbit at 760 km altitude, the corresponding Δv is 0.52 m/s.

Engaging the laser from a distance of 1600 km, with the same hypotheses as previously mentioned ($\eta = 0.8$, $\Phi = 8.5$ kJ/m²), considering a 1 ton debris, it would require 2k pulses of 3.2 kJ over 830 s, with a Pulse Repetition Frequency of 2.4 Hz. It can of course be done in several paths; over one day, there can be more than 10 occurrences for such operations.

4. Synthesis and open points

4.1. Synthesis

Table 1 synthesizes the results of our studies, applied to the 4 cases of operations identified in the paper.

This synthesis describes slightly different references compared to those presented in previous chapters, but globally it just reflects the current options under study.

Table 1
System synthesis.

Application	GEO A	GEO B	LEO nudge	LEO small
System				
Mass (kg)	5000	5000	5000	6000
Range (km)	10	2400	1600	250
Primary mirror diameter (m)	0.3	3	3	3
Spot size on target (m)	0.27	1.00	0.7	0.11
Average optical power (kW)	6.4	8	8	0.8
Peak pulse rep. frequency (Hz)	64	1.2	2.5	116
Pulse energy (kJ)	0.50	6.8	3.2	0.083
Cost total (M$)	212	560	220	146
Targets				
Number *N* per year	10	10	1	1.E+05
Time to complete operation on 1	30 h	3 mos	1 day	10 s
Time to complete operation on *N*	1 yr	3 mos		5 mos
Mass (kg)	3000	3000	1000	0.05
Illumination duration per stage (h)	14.2	2.4	830	10
Δv (m/s) total per stage	10.9	1.82	–	–
Δh (km) per phase of two stages	–	100	–	–
Δh (km) total	300	300	2	−560
Δv (m/s) total	10.9	10.9	0.52	−157

The parameters common to all 4 simulations are a pulse duration $\tau = 100$ ps, a wavelength $\lambda = 355$ nm, a fluence $\Phi = 8.5$ kJ/m² deposited on the target, and a coupling coefficient $C_m = 100$ N/MW.

The mass and cost evaluations have been done by Photonic Associates, LLC internal tools, not by CNES.

4.2. Open points

Numerous aspects have to be looked at in more depth, even though none of them appear critical enough to endanger the concept.

1. The plasma ejection is roughly perpendicular to the impacted surface, which means that one has to take into account the effective orientation of the target. Several studies [31,33] have looked in depth at this effect, showing that it can be translated in a slightly overall efficiency, but globally, even if wrongly oriented, an impulse in a counter-velocity direction always lead to a semi-major axis reduction for the target.
2. The impulses should not generate a tumbling movement of the target. To avoid this, the selected impact zone shall be such that it annihilates any angular movement; a closed loop control of the laser taking into account the observed movement of the target is necessary.
3. There is a need for more experimental data on a larger set of materials, representative of the targets mentioned here. The small debris should be in their vast majority Aluminum or Carbon derived, for which plenty of data is already available, but for large integral satellites or rocket-bodies, some additional information may be required to take into account thermal protections, MLI, paints, etc. This need for data is especially acute for schemes using lasers with tens of kHz pulse repetition rate.
4. A global simulation of the cleaning of the GEO ring should be performed, taking into account the real orbital data of the real debris, associated to an optimization tool, derived from the travel salesman problem, in order to have a clear evaluation of the performance of the system, in both options.

5. Conclusions

The orbital debris problematic may become a serious concern in the coming years, both in LEO and in GEO although for different reasons, whatever the size of the debris.

Numerous solutions have been identified and published, such as the Active Debris Removal of large spacecraft and rocket bodies in LEO, and several demonstration missions have been decided.

Collision avoidance between large operational maneuverable satellites and cataloged debris is applied throughout the world, activity highly developed since the collision between Iridium 33 and Cosmos 2251 in 2009.

Shielding of critical satellites is an efficient way to minimize the effect of smaller debris impact.

Nevertheless, there are some potential threats which do not yet have solutions, such as the protection of LEO satellites from small uncatalogued debris, collision avoidance in LEO between non maneuverable large debris, or cleaning the orbital slots in GEO, removing derelict large spacecraft from very valuable zones.

The concept proposed here, an orbital laser debris remover functioning in UV band, delivering very high intensity very short pulses, appears to be well adapted as a solution to cover these open challenges, with reasonable size, mass, power budget, based on a relatively important experimental data base.

Appendix 1. Laser orbit modification

For an orbit, energy per unit mass

$$h = \left[\frac{v^2}{2} - \frac{MG}{r}\right] \tag{A1.1}$$

with velocity v, geocentric radius r and gravitational potential constant MG. Velocity in a circular orbit is

$$v = \sqrt{MG/r} \tag{A1.2}$$

Differentiating (A.1.2), the impulsive Δv required to modify this orbit to achieve a new semi-major axis value a is given by

$$\Delta v = \lim_{a \to r}\left[\frac{MG}{2v}\frac{\Delta a}{a^2}\right] = \frac{\sqrt{MG}}{2r^{1.5}}\Delta a = \frac{\eta C_m \Phi}{\mu} \tag{A1.3}$$

equal to the laser impulse delivered by on-target laser fluence Φ (J/m^2) operating with momentum coupling

coefficient C_m (N s/J) for a target with mass density μ kg/m^2. Impulse transfer efficiency η is taken to include the combined effects of improper thrust direction on the target, target shape effects and tumbling in reducing the efficiency of producing a desired vector velocity change antiparallel to the target track.

In a single impulsive transfer, it is important to recall that the magnitude of perigee or apogee change is twice Δa.

$$\Delta a = |\Delta r_{p,a}/2| \tag{A1.4}$$

The new velocity is

$$v'^2 = MG\left[\frac{2}{r} - \frac{1}{a'}\right] \tag{A1.5}$$

N pulses delivering a total fluence

$$N\Phi = \frac{\sqrt{MG}\mu\Delta r_{p,a}}{4\eta C_m a^{1.5}} \tag{A1.6}$$

to the target in the appropriate direction during an interval short enough to qualify as a single impulse will produce the desired change of perigee or apogee.

Otherwise, to create a new circular orbit Δr higher or lower, total fluence $2N\Phi$ is required.

Whether applied by one or two stations, GEO re-orbit is the latter case, requiring $2N\Phi$ J/m^2 total, twice that shown in Eq. (A1.6).

Appendix 2. Small Fresnel Number focusing

The "Fresnel Number" (Please note, $F \neq \Phi$)

$$F = w^2/(L\lambda) \tag{A2.1}$$

See Appendix Fig. A2.1

For many of our cases, both the focusing aperture and its focal plane are in the near field where F is small. For example, if $\lambda = 0.35$ μm, range L to the target surface = 1000 km and aperture clear radius $w = 1$ m, $F = 2.9$.

The classic expression

$$w_{os} = \lambda L/(\pi w) = w/(\pi F) \tag{A2.2}$$

for the spot radius of a perfect Gaussian beam depends upon the opposite, far-field assumption, $F >> 1$, where the geometrical focus does coincide with that predicted by propagation theory This says that beam size expands with distance z from the beam waist (best focus) according to [34]:

$$w^2(z) = w_o{}^2 + (\theta z)^2 = w_o{}^2\left[1 + (z/z_R)^2\right] \tag{A2.3}$$

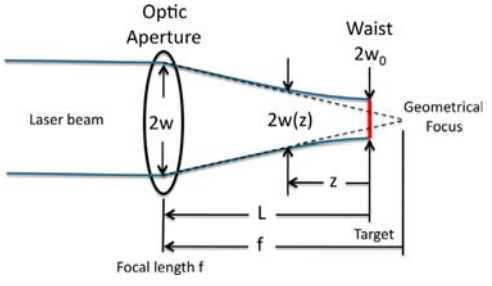

Fig. A2.1. Focusing a laser beam using an optic with aperture 2w.

where $\theta = \lambda/(\pi w_o)$ and the "Rayleigh Range" at which $w = \sqrt{2}w_o$ and intensity is half maximum,

$$z_R = \pi w_o{}^2/\lambda \tag{A2.4}$$

The solution to the resulting quadratic is given by

$$\frac{w_o^2}{w^2} = \frac{1}{2}\left[1 \pm \sqrt{1 - \left(\frac{2\lambda z}{\pi w^2}\right)^2}\right] \tag{A2.5}$$

and we normally take the negative root. With $z = L$, we can see that (A2.4) amounts to

$$\frac{w_o^2}{w^2} = \frac{1}{2}\left[1 \pm \sqrt{1 - \left(\frac{2}{\pi F}\right)^2}\right] \tag{A2.6}$$

making it obvious why (A2.2) is inaccurate for small F. Eq. (A2.5) can be re-expressed in the form [35]

$$\left[1 - \frac{2w_o^2}{w^2}\right]^2 = 1 - \left(\frac{2w_{os}^2}{w^2}\right)^2. \tag{A2.7}$$

and w_{os} is defined in Eq. (A2.2). This relationship is plotted in Fig. A2.2, which shows both roots of (A2.5), only the upper one of which is normally useful. For long-range laser interaction in space, the mirror size and weight are critical elements, and one frequently finds that the projection aperture diameter $D = 2w$ is of the same order as the laser spot size $d_s = 2w_o$ on target. Then, F is small and the whole problem is carried out in the near field of the transmitting aperture [36].

Fig. A2.2 shows Eq. (A2.2) accuracy degrading significantly as $z \to z_R$. The upper branch of Fig. A2.2 is the best we can do to transform a plane wave at the focusing optic input into an intensified plane wave at the target over a large distance. We can always obtain $L = 2z_R$ by letting the beam re-expand to its original size at the target. For $\lambda = 0.35$ μm, for example, with a 2 m diameter mirror, $2z_R = 17{,}950$ km. Table A2.1 shows the significance of these errors for a problem typical of the set we consider here.

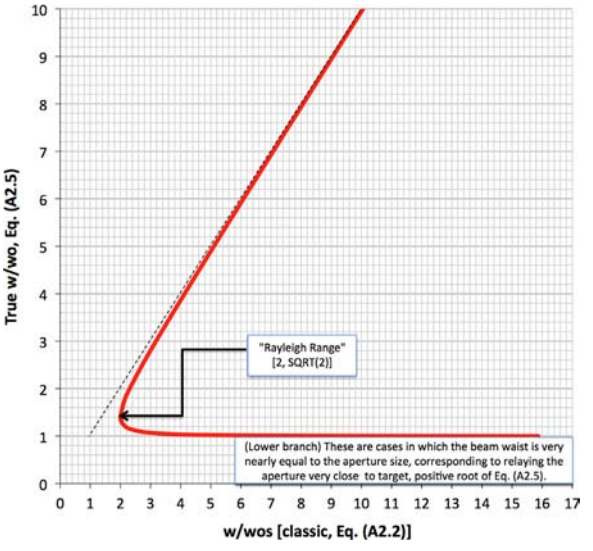

Fig. A2.2. Beam waist errors (Eq. (A2.7)).

Table A2.1
Near-field error.

Wavelength λ (μm)	0.35
Range L (km)=z_R (km)	8,980
Aperture radius w (m)	1
Fresnel number F	0.32
Classic w_o^2 (Eq. (A2.2))	1.00
True w_o^2 (Eq. (A2.5))	0.50
Error in focus area	100%

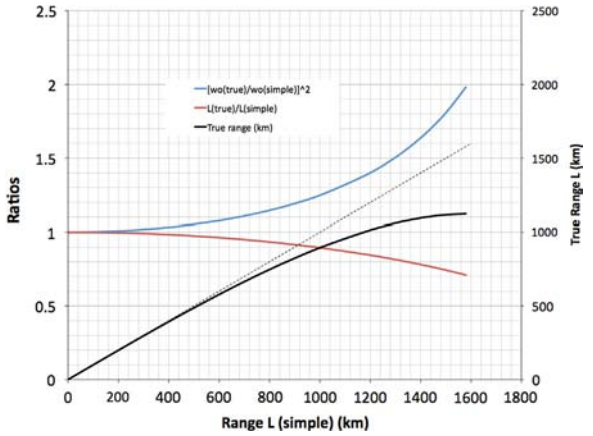

Fig. A2.3. Beam waist and range errors for the case w=1 m, λ=0.35 μm.

If we turn this around and use (A2.2) to determine range, Fig. A2.3 shows the error that results, as well as the beam waist error, for 0.35 μm wavelength. The true focus is always closer than the geometrical one.

We note that a reasonable approximation to the results of Eq. (A2.5) for quick estimates is given by

$$\frac{1}{d_s^2} \simeq \frac{1}{d_o^2} - \frac{2}{D^2} \tag{A2.8}$$

where $D=2w$, $d_s=2w_o$ and $d_o=2w_{os}$.

The foregoing is all for perfect single mode Gaussian beams. Now, we need to include the effects of imperfect beam quality with a quality factor $M^2>1$ and possible non-Gaussian shapes. We are normally interested in diameters, not radii, so we obtain Eq. (2) in the main text,

$$r_o = (a/2)M^2 L\lambda/D = \frac{2M^2\lambda L}{\pi D} \tag{A2.9}$$

for a Gaussian beam and multiply the results we obtain from (A2.5) for w_o by aM^2 (Table A2.2).

The "beam quality factor" M^2 is often loosely defined in use and understood to be "number of times diffraction limited" of the focal spot, although it has been defined carefully [37]. The parameter M describes the electric field, so that intensity quality is described by M^2, and λ is replaced everywhere in Eqs. (A2.1)–(A2.5) by $M^2\lambda$.

Table A2.2
Beam quality factors *a*.

Gaussian	$4/\pi$=1.27
HyperGaussian (index 6)	1.7
Airy (hard aperture)	2.44

Table A3.1
Laser system TRL's and references.

System	TRL	Ref.
Monolithic diode pumped solid state single pulse	8	[42]
Monolithic diode pumped solid state repetitive pulse	6	[40]
Modelocked, phased low intensity CW fiber, N=64	5	[44]
Modelocked, phased femtosecond pulse fiber array, N=2–4	4	[45,46]
Modelocked, phased femtosecond pulse fiber array, N=10k	2	–

Appendix 3. System issues

TRL's for monolithic diode pumped solid state lasers (DPSSLs) vs. massively parallel fibers

Table A3.1 provides our estimates of the comparative Technology Readiness Levels [38] of various alternatives for the pulsed laser required in the system described in this paper.

High power diode pumped solid state laser (DPSSL) technology is now mature. 25 kW CW lasers are routine. In the second category, repetitively pulsed lasers in Table A3.1, notable are the Livermore MERCURY laser, the Livermore HAPLS laser, due to be shipped to Prague next year for use with the European ELI extreme light facility and the CLF DiPOLE laser in the UK. Until its disassembly for use with HAPLS, MERCURY provided 300 k shots of 50 J, 15 ns pulses at 10 Hz. HAPLS will produce 30 J, 10 Hz pulses at 30 fs duration. ELI will extend this to 50 J, 10 Hz. DiPOLE now makes 10 J, 10 ns pulses at 10 Hz, and is being expanded to 1 kJ per pulse capability. Typical references are given in the Table.

We are not aware of any experimental demonstration of phased modelocked nanosecond pulse fiber laser arrays with thousands of fibers. When successful, this approach is clearly the best because of easy heat dissipation system design, high gain efficiency (leading to low pump power) and considerable infrastructure for single fibers in telecom applications. Problems are the difficulty of controlling phase in nonlinear materials on very short intervals, and severe limitation of pulse energy per fiber due to strong optical nonlinearity to the order of 1 mJ per fiber [39].

DPSSL system efficiency

Table A3.2, adapted from [31] is assumed system efficiencies of a monolithic third harmonic conversion DPSSL, with appropriate references, working backward from 8 kW time-average 3rd harmonic output power, composed of 3 kJ, 2.5 Hz, 100 ps pulses. The system described in this paper is characterized by less demanding requirements than that in [31].

Table A3.2
Estimated DPSSL system parameters.

Output wavelength	355	nm	
Pulse energy, maximum (kJ)	3.2	kJ	
Pulse duration	100	ps	
PRF	2.5	Hz	
Output optical power	8.0	kW	
1st to 3rd harmonic conversion efficiency	0.8		[43]
Diodes to 1st harmonic conversion efficiency	0.53		[41,42,47]
Laser diode electrical to optical (e-o) efficiency	0.6		[48]
Overall laser e-o efficiency	0.25		
Resulting laser electrical input	31	kW	
Heat removal system	8	kW	
Laser system electrical power requirement	39	kW	
Solar array mass/area	0.85	kg/m^2	[49]
Solar array power/area	0.27	kW/m^2	[49,50]
Solar array area	160	m^2	

Large target orientation

Because the laser ablation thrust vector will always be perpendicular to the local target surface rather than necessarily counter to the laser propagation vector, we will need to orient the target for best performance. For very small targets, natural and induced tumbling will lead to an average vector pointing counter to the beam averaged over many shots, with a reduced efficiency η arising from shape effects [33]. For large targets, this inefficiency should not and need not be tolerated. The optical system will be able to resolve such targets (see for example Fig. 6) and employ an adaptive control system which points the beam off the target center of mass so as to orient the target as desired for optimum engagement.

Damage thresholds, post-shot ablation and other details

Optical damage thresholds are very well cataloged. They are thresholds, in the sense that hundreds of thousands of shots do not lead to damage below the threshold fluence.

Ref. [14] demonstrates that the actual data (which includes all the aspects of target ablation) are described by our theoretical phenomenology.

References

[1] General information on orbital debris can be found in NASA Orbital Debris quarterly news, ⟨http://orbitaldebris.jsc.nasa.gov/newsletter/newsletter.html⟩.
[2] Space track ⟨http://www.space-track.org⟩.
[3] D. McKissock, JSpOC conjunction assessment process, in: Proceedings of the 1st International Conjunction Assessment Workshop, CNES, Paris, 19–20 May 2015.
[4] M. Moury, CAESAR-conjunction assessment with Middle Man, in: Proceedings of the 1st International Conjunction Assessment Workshop, CNES, Paris, 19–20 May 2015.
[5] D. Kessler, Collisional cascading: the limits of population growth in low Earth orbit, Adv. Space Res. 11 (12) (1991) 63–66.
[6] C. Bonnal, et al., Active Debris Removal: recent progress and current trends, Acta Astronaut. 85 (2013) (2013) 51–60.
[7] General information on Active Debris Removal can be found, in: Proceedings of the 3rd European Workshop on Space Debris Modelling and Remediation, CNES, Paris, 18–20 June 2014.
[8] D. Mc Knight, et al., System engineering analysis of derelict collision prevention options, Acta Astronaut. 89 (2013) (2013) 248–253.
[9] J. Carroll, Can pulsed laser ablation prevent most debris creation IAC-14, A6.P.52, Toronto, September 29–October 3 2014.
[10] IADC Protection manual, downloadable at ⟨http://www.iadc-online.org⟩.
[11] T. Flohrer, 16th issue of classification of geosynchronous objects ESA GEN-DB-LOG-00126-HSO-GR, 27 February 2014.
[12] I. Retat, The development status of "Roger" IAC-13, A6.5 2012, Naples, 1–5 October.
[13] A. Kantrowitz, Proceeding of SDIO/DARPA Workshop on Laser Propulsion, Vol. 2, 1986, p. 1.
[14] C. Phipps, et al., Impulse coupling to targets in vacuum by KrF, HF, and CO_2 single-pulse lasers, J. Appl. Phys. 64 (3) (1988) 1083–1096.
[15] C. Phipps, LISKBROOM: a laser concept for clearing space junk, in: Proceedings of the AIP Conference, 318, 1994, 466-468.
[16] W. Schall, Orbital debris removal by laser radiation, Acta Astronaut. 24 (1991) 343–351.
[17] C. Phipps, et al., ORION: clearing near-Earth space debris using a 20-kW, 530-nm, Earth-based, repetitively pulsed laser, Laser Part. Beams 14 (1) (1996) 1–44.
[18] J.W. Campbell, Project orion: orbital debris removal using ground-based sensors and lasers, NASA-TM-108522, October 1996.
[19] C. Jacquelard et al., CLEANSPACE small debris removal by laser illumination and complementary technologies, in: Proceedings of the 3rd European Workshop on Space Debris Modeling and Remediation, 5.1, CNES, Paris, 18–20 June 2014.
[20] J. Stupl, Lightforce photon-pressure collision avoidance: efficiency assessment on an entire catalogue of space debris, in: Proceedings of AMOS Technical Conference, 2013.
[21] S. Shen, Cleaning space debris with a space-based laser system, Chin. J. Aeronaut. 27 (2014) 805–811.
[22] M. Schmitz, et al., Performance model for space-based laser debris sweepers, Acta Astronaut. 115 (2015) 376–383.
[23] A. Rubenchik et al., Laser systems for orbital debris removal, in: Proceedings of AIP Conference, 1278, 347, 2010.
[24] C. Phipps, et al., Removing orbital debris with lasers, Adv. Space Res. 49 (2012) 1283–1300.
[25] R. Soulard, et al., ICAN: a novel laser architecture for space debris removal, Acta Astronaut. 105 (1) (2014) 192–200.
[26] T. Ebisuzaki, et al., Demonstration designs for the remediation of space debris from the International Space Station, Acta Astronaut. 112 (2015) 102–113.
[27] Proceedings of the Workshop Laser solutions for Orbital Debris, Paris, 27–28 April 2015. ⟨http://www.izest.polytechnique.edu/izest-home/izest-events/042015-1st-workshop-on-laser-solutions-for-orbital-space-debris/⟩.
[28] C. Phipps, et al., Laser impulse coupling at 130 fs, Appl. Surf. Sci. 52 (2006) 4838–4844.
[29] J. Sinko, C. Phipps, Modeling CO_2 laser ablation impulse of polymers in vapor and plasma regimes, Appl. Phys. Lett. 95 (2009) 131105-1–131105-3.
[30] M. Quinn et al., ICAN: a novel laser architecture for space debris removal, P.4.1, in: Proceedings of the 3rd European Workshop on Space Debris Modeling and Remediation, CNES, Paris, 18–20 June 2014.
[31] C. Phipps, L'ADROIT – a space borne ultraviolet laser system for space debris clearing, Acta Astronaut. 104 (2014) 243–255.
[32] E. Köse, R. Perline, Double-mirror catadioptric sensors with ultra wide field of view and no distortion, Appl. Opt. 53 (2014) 528–536.
[33] D. Liedahl, et al., Pulsed laser interactions with space debris: target shape effects, Adv. Space Res. 52 (5) (2013) 895–915.
[34] H. Kogelnik, T. Li, Laser beams and resonators, Appl. Opt. 5 (1966) 1550–1567.
[35] J. Sollid, C. Phipps, S. Thomas, E. McLellan, Lensless method of meausuring Gaussian laser beam divergence, Appl. Opt. 17 (1978) 3527–3529.
[36] W.H. Carter, Focal shift and concept of effective Fresnel number for a Gaussian laser beam, Appl. Opt. 21 (1982) 1989–1994.
[37] A.E. Siegman, How to (Maybe) measure laser beam quality", in: Proceedings of Tutorial Presentation at the Optical Society of America Annual Meeting Long Beach, California, 1997, p. 9.
[38] ⟨http://esto.nasa.gov/files/trl_definitions.pdf⟩.
[39] ⟨http://www.rp-photonics.com/mode_locked_fiber_lasers.html⟩.

[40] S. Banerjee, et al., High-efficiency 10 J diode pumped cryogenic gas cooled Yb:YAG multislab amplifier, Opt. Lett. 37 (2012) 2175, http://dx.doi.org/10.1364/OL.37.002175.
[41] A.J. Bayramian et al. Fusion Sci. Tech. vol. 52, 2007, p. 383.
[42] A. Bayramian, A. Erlandson, Comparison of Nd:pho sphate glass, Yb:YAG and Yb:S-FAP laser beamlines for laser inertial fusion energy, LLNL-PRES-581113 2012. ⟨https://lasers.llnl.gov/workshops/hec_dpssl_2012/pdf/9-13-12/A.Erlandson.pdf⟩.
[43] D. Neely, Rutherford Appleton Laboratory UK, Private communication, 2014.
[44] J. Bourderionnet, et al., Collective coherent phase combining of 64 fibers, Opt. Express 19 (2011) 17053–17058.
[45] L. Daniault, et al., Coherent beam combining of two femtosecond fiber chirped-pulse amplifiers, Opt. Lett. 36 (2011) 621–623.
[46] A. Klenke, 539 W, 1.3 mJ, four-channel coherently combined femtosecond fiber chirped-pulse amplification system, Opt. Lett. 38 (2013) 2283–2285.
[47] A. Bayer, et al., Scalable and modular diode laser architecture for fiber coupling that combines high-power, high-brightness and low weight, Photonics West, 2014.
[48] J. Noekum, Overview on new diode lasers for defense applications, in: Proceedings of SPIE Europe Security and Defense, 2012. ⟨http://spie.org/x4304.xml⟩.
[49] M. Haag, BEPI-COLUMBO: lightweight fiber-coupled diode laser pump module for the BepiColumbo laser altimeter, in: Proceedings of the 2nd ESA-NASA Working Meeting on Optoelectronics, Noordwijk, Netherlands, 2006.
[50] N. Fatemi, et al., Solar array trade studies between very high efficiency multi-junction and Si space solar cells, in: Proceedings of the 28th IEEE PVSC, Anchorage, Alaska, 2000.